A DUAL-BAND 3-BIT RECONFIGURABLE INTELLIGENT SURFACE WITH INDEPENDENT CONTROL OF PHASES

Jing Cheng Liang[1], Wen Hua Gao[1], Jun Yan Dai[1,2,3], Peng Zhang[4], Qiang Cheng[1,2,3], and Tie Jun Cui[1,2,3]

[1]State Key Laboratory of Millimeter Waves, Southeast University, Nanjing 210096, China, [2]Institute of Electromagnetic Space, Southeast University, Nanjing 210096, China, [3]Frontiers Science Center for Mobile Information Communication and Security, Southeast University, Nanjing 210096, China, [4]Shenyang Aircraft Design Institute

NOTE: Corresponding author: Jun Yan Dai, junyand@seu.edu.cn; Peng Zhang, zhangpengshenfei@163.com; Qiang Cheng, qiangcheng@seu.edu.cn; and Tie Jun Cui, tjcui@seu.edu.cn

Abstract *– Reconfigurable Intelligent Surfaces (RISs) have received a great deal of attention from the wireless communication community due to their powerful ability to improve the wireless communication environment. Dual-band RIS enables aperture to share two bands, improving spectrum utilization in wireless communications and thus expanding communication capacity. However, most of the reported dual-band RISs cannot achieve independent controls of the dual-band phases, which greatly limits their practical application in wireless communications. In this paper, we propose a dual-band 3-bit RIS to achieve independent controls of the reflection phases in two frequency bands by designing two tunable structures without raising the profile. It also exhibits low sensitivity to incident angles between 0° and 50°. Thereafter, the beam steering ability of the proposed RIS is further investigated with experiments under normal and oblique incidences at two frequencies, which demonstrates the powerful potential of RISs to manipulate the electromagnetic wave propagation environment.*

Keywords – Angular stability, beam steering, dual-band, reconfigurable intelligent surface

1. INTRODUCTION

Future wireless communications are featured by increasing the demands for communication speed, capacity and stability. Originating from programmable and information metasurfaces [1, 2, 3, 4, 5, 6], reconfigurable intelligent surfaces (RISs) are widely recognized as one of the most promising frontier technologies for next-generation wireless communications because of their ability to flexibly modulate Electromagnetic (EM) waves [7, 8, 9, 10] in real time, including the amplitude [11], phase [12], polarization [13] and frequency [14]. They enable active and intelligent controls of the EM environment, thereby breaking the inherent notion that wireless channels are randomly uncontrollable [15, 16].

Multichannel signals are transmitted independently and simultaneously in the same wireless environment by manipulating the EM waves independently on two or more frequency bands, thus increasing the communication capacity without enlarging the RIS aperture size [17, 18]. Some approaches on dual-band RISs [17, 19, 20, 21] have been proposed, but their reflection phases cannot be independently modulated on both bands. Hence such dual-band RISs cannot fully exploit their advantages in wireless communications. A 1-bit dual-band RIS element loaded with two PIN diodes in different layers has been proposed in [22]. However, the longer bit-width RISs can achieve finer manipulation of EM waves and higher wireless channel capacity [12, 23]. In addition, the potential phase distortion caused by different incidence angles also needs to be considered, since it is difficult to obtain a normal incidence scenario in the real wireless communication environment [16, 24].

In this paper, a dual-band 3-bit RIS is proposed to achieve independent control of the reflection phase in two frequency bands (FB_1=2.52-2.67 GHz, FB_2=3.4-3.5 GHz). The angular stability of the RIS has been improved by designing numerous metallic vias between the elements. Beam steering is performed to demonstrate the ability of our proposed RIS to manipulate the far-field EM wave distribution. In addition, the scattering patterns are investigated at two frequencies for both normal and oblique incidences. Finally, the measurement results of the fabricated prototype are in good agreement with the theoretical and simulation

results. The proposed dual-band RIS has a powerful ability in EM wave manipulation, thereby possessing great potential for future RIS-assisted wireless communication.

2. THE DESIGN PROCEDURE AND SIMULATION OF THE RIS ELEMENT

Fig. 1 shows the structure of the proposed dual-band RIS element. It is composed of three metal layers and two dielectric slabs (F4B, $\varepsilon_r = 2.65$, $\tan\delta = 0.003$) with a thickness of h_1 (3.3 mm) and h_2 (0.2 mm), respectively. The top metal layer consists of two different pairs of metal patches, each of which is connected by a varactor to realize EM wave manipulation in different frequency bands. The design of the rectangular patches in the RIS element is inspired by [12] and [22]. The dimensions of the

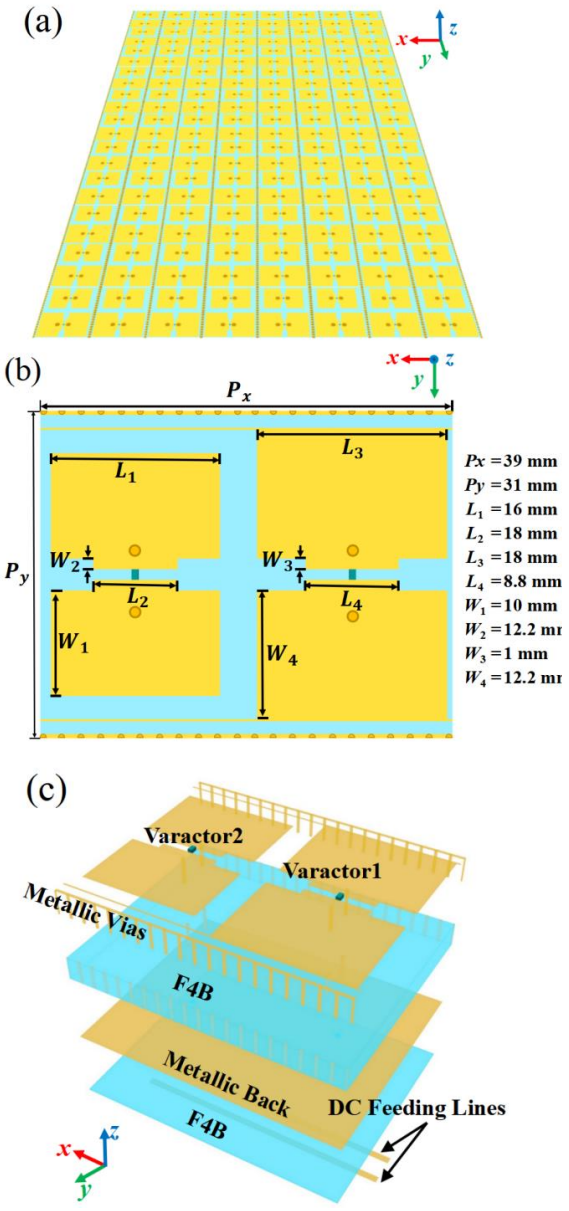

Fig. 1 – Sketch of the proposed (a) RIS and (b) the top view and (c) the explosive view of the RIS element

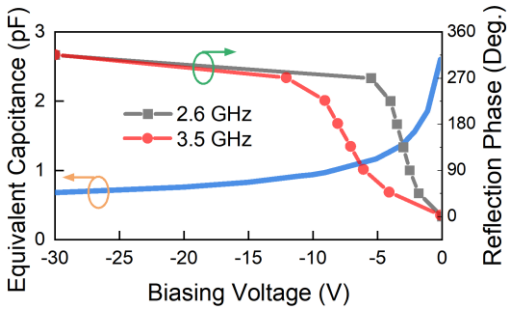

Fig. 2 – The equivalent capacitance of the varactor and the reflection phase varies with biasing voltage

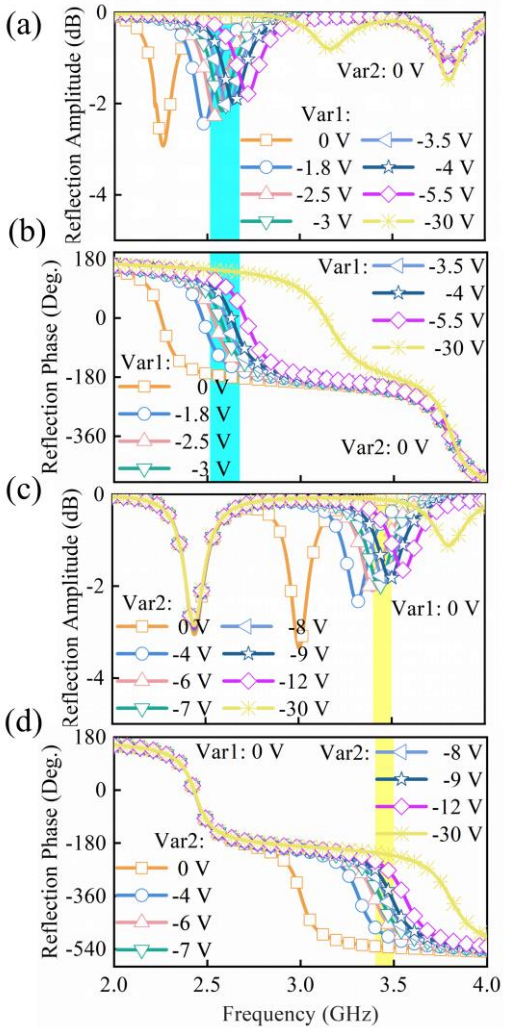

Fig. 3 – The simulated reflection spectrum of the RIS element at normal incidence. (a) Amplitude and (b) phase spectrum operating in FB_1 (2.52-2.67 GHz). (c) Amplitude and (d) phase spectrum operating in FB_2 (3.4-3.5 GHz)

Table 1 – The 3-bit coding states and corresponding voltages of the varactors

Coding States	0	1	2	3	4	5	6	7
Voltage (V) on Var1	0	−1.8	−2.5	−3	−3.5	−4	−5.5	−30
Phase shift in FB_1 (2.52-2.67 GHz)	0°	45°	90°	135°	180°	225°	270°	315°
Voltage (V) on Var2	0	−4	−6	−7	−8	−9	−12	−30
Phase shift in FB_2 (3.4-3.5 GHz)	0°	45°	90°	135°	180°	225°	270°	315°

rectangular patches can be easily adjusted to optimize the EM characteristics of the RIS. At the resonant frequency, the induced current is excited on the surface of the rectangular patches and flows through the varactor, thus allowing the varactor to control the scattering field. The varactor (Skyworks 1405-079LF) can be modeled as a series circuit of a tunable capacitor (C_{var} = 0.66~2.6 pF), a resistor (R_{var} = 0.7 Ω), and an inductor (L_{var} = 0.7 nH). The varactor with a small equivalent resistance is selected to reduce the ohmic loss, whose equivalent capacitance can be varied with the biasing voltage, as shown in Fig. 2. The middle metal layer acts as a reflecting plate; meanwhile, it also connects to the patches through metallic vias to work as the Direct Current (DC) ground. The two bottom feeding lines are connected to the surface patches to provide independent control voltages for varactors. Since each feeding line connects all the elements along the x-axis direction, it leads to them working in the same state. Numerous metallic vias are designed in the upper substrate along the *x*-axis to suppress the adjacent coupling effect and form a more stable EM wave propagation mode, thus reducing the dependence of the incident angles, as described in [12].

During the simulation, the commercial EM calculation software, CST Microwave Studio 2019, is used to calculate the reflection coefficient of the RIS element under plane wave illumination. The unit cell boundaries are set on the *x* and *y* axes to simulate an infinite array, which considers the mutual coupling between the adjacent elements. The Floquet port is set above the element to excite *y*-polarized plane waves.

Fig. 3 shows the reflection amplitude and phase of the RIS element under different biasing voltages at normal incidence. The blue and yellow bars respectively represent the two bands independently controlled by varactor1 (Var1) and varactor2 (Var2). For example, when the voltage on Var2 is fixed (0 V),

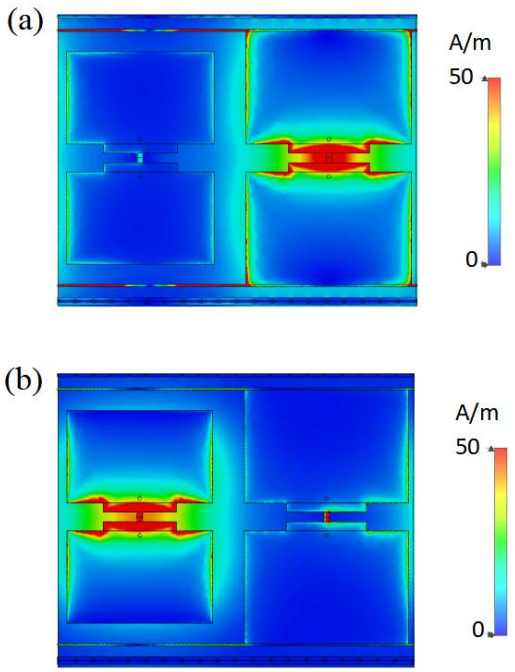

Fig. 4 – The surface current distribution of state '3' on the patches in (a) FB_1 and (b) FB_2

the reflection phase in FB_1 will vary with the voltage on Var1, while the reflection phase in FB_2 remains stable, as shown in Fig. 3(b); and vice versa Fig. 3(d) shows that the reflection phase in FB_2 only depends on the control voltages on Var2. In addition, a reflection amplitude above –3 dB can be achieved under different biasing voltages, as shown in Fig. 3(a) and Fig. 3(c).

A phase-shifting RIS can be defined as an *n*-bit quantized RIS that has 2^n coding states with phase shifting intervals of $360°/2^n$ [1]. The designed RIS element has the capability of continuous phase shifting in both FB_1 and FB_2 with the maximum phase shifting range exceeding 315°, thereby evolving into a dual-band 3-bit RIS. Table 1 lists the required biasing voltages for the coding states ("0, 1, 2,..., 7") in two frequency bands FB_1 and FB_2, respectively.

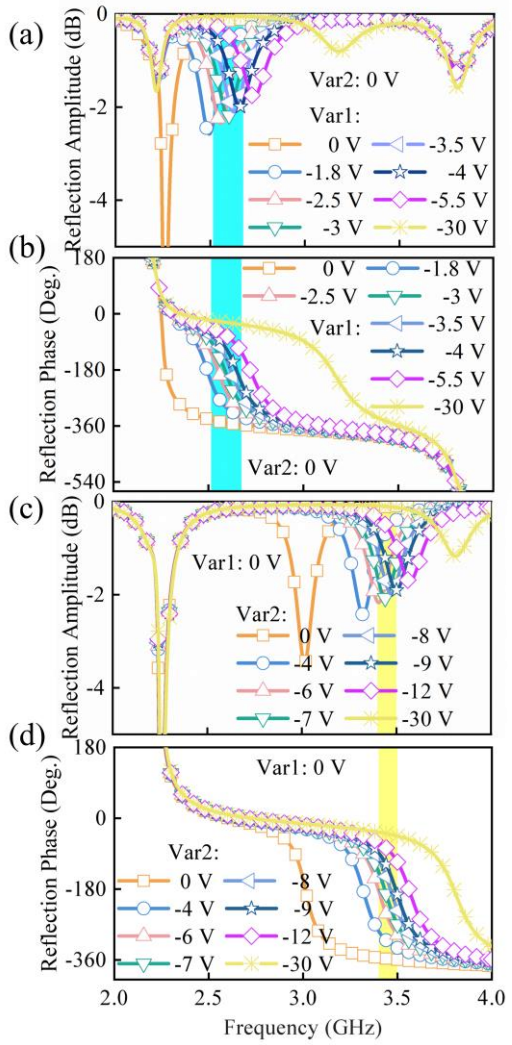

Fig. 5 – The simulated reflection spectrum of the RIS element at TM oblique incidence of 50°. (a) Amplitude and (b) phase spectrum working in FB_1. (c) Amplitude and (d) phase spectrum working in FB_2

To explain the working mechanism of the designed dual-band RIS element, field monitors are set respectively at 2.6 GHz and 3.4 GHz in the numerical simulation to observe the distribution of the surface current $\boldsymbol{J_s}$. Fig. 4(a) and Fig. 4(b) show the surface current distribution of state '3' on the patches in FB_1 and FB_2, respectively. It can be observed that $\boldsymbol{J_s}$ is mainly concentrated near Var1 when the element operates in FB_1, while $\boldsymbol{J_s}$ is mainly concentrated near Var2 when the element operates in FB_2. This allows the varactors to control the EM wave reflection independently in the dual bands.

In the actual wireless communication environment, both users and base stations are usually located away from the RIS normal, indicating that oblique incidence is more common. However, when oblique incidence occurs, the distortion of the reflection phase and amplitude caused by the incident angle may lead to performance deterioration of the RIS-assisted wireless communication system. In addition, it has been pointed out that the angle-dependent RIS may lead to non-reciprocity between the incident and reflected angles [16, 24]. Therefore, the robustness of RIS EM responses to the incident angle is a very important indicator to measure the performance of the RIS-assisted wireless communication system.

To demonstrate the angular property of the element, the reflection spectrum at a TM oblique incidence of 50° is further studied. As shown in Fig. 5, in the two separate operating bands, the reflection amplitudes of -3 dB or more can still be achieved, as well as the eight coding states with equal phase differences. Compared with Fig. 3, the reflection responses show low sensitivity to the incident angle. However, they still deteriorate when the incident angle becomes large. In fact, the performance of RIS at larger incidence angles will be influenced by many factors. For example, the limited aperture and the truncated boundary effect of the RIS make it unsuitable to work at a large oblique incident angle. For a TE polarized oblique incidence, we can also obtain angular stability from 0° to 50°. However, since the metallic vias parallel to the x-axis has no effect on the TE oblique incidence, the stability of the reflection coefficient is slightly worse for the TE oblique incidence than for the TM oblique incidence.

3. BEAM STEERING OF THE RIS

When an extra phase gradient is generated on the RIS interface, the EM wave will be abnormally reflected. According to the generalized Snell's law [25], the reflection angle is determined by the phase gradient, incidence angle and operating frequency:

$$\theta_r = sin^{-1}\left(\frac{\lambda_0}{2\pi}\cdot\frac{d\phi}{dx} + sin\,\theta_i\right) \quad (1)$$

where θ_i and θ_r are the incidence and reflection angles with respect to the RIS normal, respectively. λ_0 is the wavelength of the EM wave in vacuum. $\frac{d\phi}{dx}$ is the phase gradient along the RIS interface. For the RIS with a finite size, we employ the scattering patterns to accurately analyze the distribution of EM waves in the far field [25, 26]:

$$f(\theta) = \sum_n^N f_n(\theta)\cdot e^{-j\varphi_0}\cdot e^{-j\frac{2\pi d}{\lambda_0}\left(n-\frac{1}{2}\right)(\sin\theta_i+\sin\theta)} \quad (2)$$

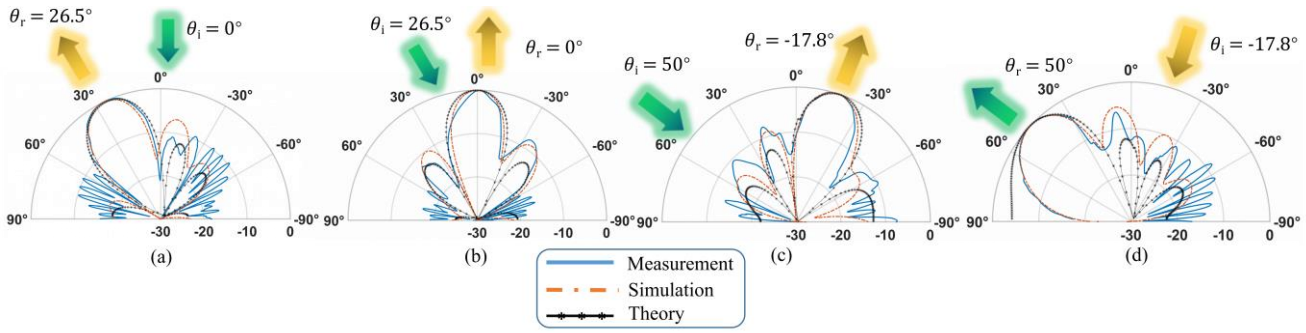

Fig. 6 – The scattering patterns at 2.6 GHz with TM incidence angles of (a) 0°, (b) 26.5°, (c) 50°, (d) –17.8°

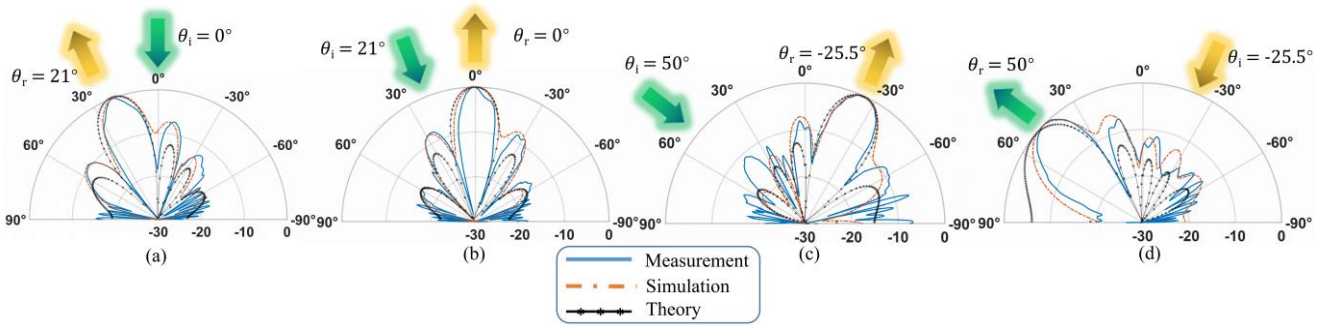

Fig. 7 – The scattering patterns at 3.4 GHz with TM incidence angles of (a) 0°, (b) 21°, (c) 50°, (d) –25.5°

where N *is* the column number of the RIS, $f_n(\theta)$ is the scattering pattern of the n-th element, which is approximated by a cosine function ($f_n(\theta) \approx \cos\theta$) [26], φ_0 is the scattering phase of the n-th element, d is the period of the RIS element. Equations (1) and (2) demonstrate the modulation principle of the reflected beam by changing the coding pattern on the RIS.

To investigate the beam steering capability of the RIS, the scattering patterns of the array composed of 8×11 elements are simulated by CST and calculated using Eq. (2). The coding sequence on the RIS is set to be "01234567" along the y-axis direction. The coding states and corresponding voltage can be found in Table 1.

As shown in Fig. 6(a), when the 2.6 GHz EM wave is normally incident on the RIS, a large lobe appears near 26.5°. This means that most of the incident energy is reflected to 26.5° by the coded RIS. When the EM wave incident is from 26.5°, the same phase gradient reflects the beam back to 0°, as shown in Fig. 6(b). The reciprocity of incident and reflection angles ensures the reciprocity of the wireless channel, which is the foundation of some wireless communication systems, such as a TDD wireless communication network [24]. The reciprocity of a wireless channel ensures the alignment of uplink and downlink in data transmission. The case of a large-angle oblique incidence has also been further considered. When the EM wave incident is from 50°, the reflected angle is –17.8°, as shown in Fig. 6(c). And when the EM wave incident is from –17.8°, the reflected angle is back to 50° again, as illustrated in Fig. 6(d). At the oblique incidence, the angular reciprocity of incidence and reflection still holds, which is attributed to the low angular sensitivity of the designed RIS element.

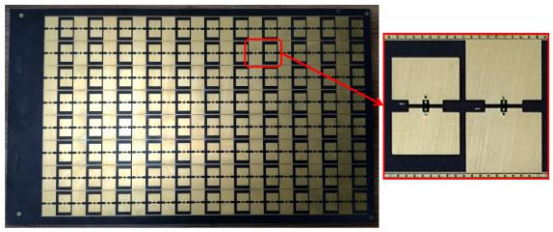

Fig. 8 – Photographs of the fabricated RIS

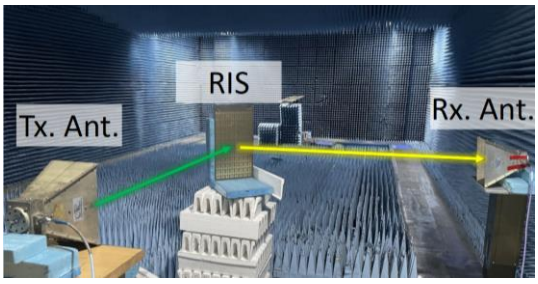

Fig. 9 – Measurement configuration of reflection coefficients

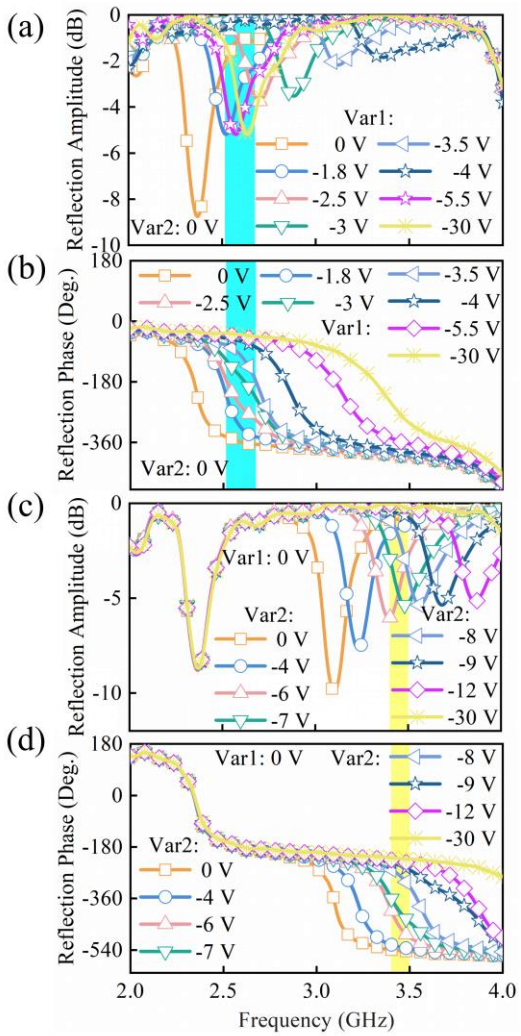

Fig. 10 – The measured reflection spectrum of the RIS element at normal incidence. (a) Amplitude and (b) phase spectrum working in FB_1. (c) Amplitude and (d) phase spectrum working in FB_2

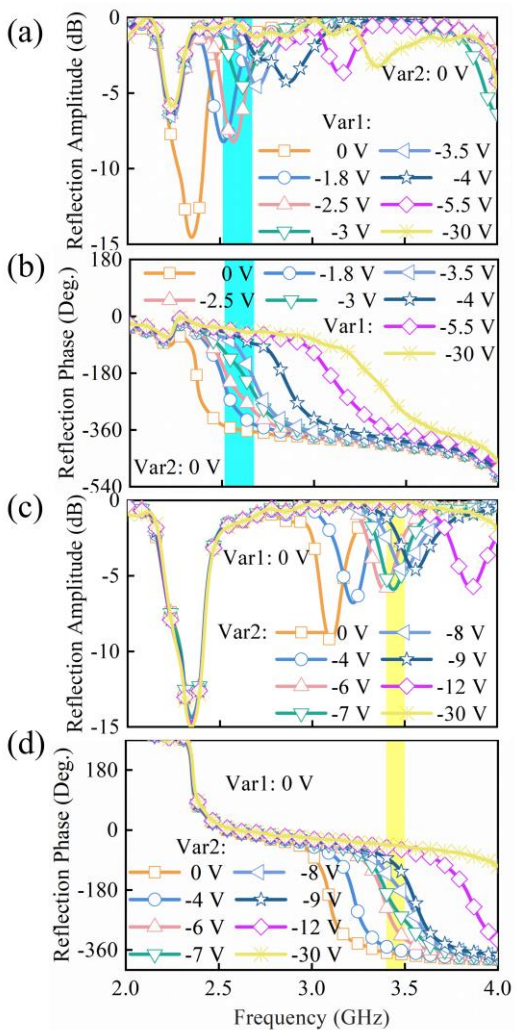

Fig. 11 – The measured reflection spectrum of the RIS element at TM oblique incidence of 50°. (a) Amplitude and (b) phase spectrum working in FB_1. (c) Amplitude and (d) phase spectrum working in FB_2

The same coding sequence "01234567" is investigated at 3.4 GHz. The corresponding 1D scattering patterns are presented in Fig. 7. Similar beam steering simulations with different oblique incidence angles confirm the angular reciprocity again. The normal incident EM waves are reflected to 21°, and the EM wave incident from 21° also returns to 0°; the EM wave incident from 50° is reflected to –25.5°, while the EM wave incident from –25.5° is reflected to 50°, consistent with the theoretical calculations.

4. FABRICATION AND MEASUREMENTS

To verify the performance of the designed RIS, a prototype is manufactured, as shown in Fig. 8. It is composed of 8×11 elements and the total size is 248×429 mm². A corresponding control circuit board is designed and fabricated to provide the biasing voltages for the varactors.

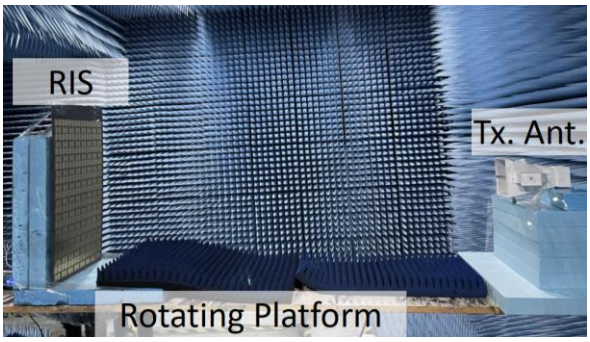

Fig. 12 – Measurement configuration of scattering patterns

Table 2 – Comparison with previous references

Reference	[12]	[17]	[19]	[20]	[21]	[22]	This work
Dual Band	No	Yes	Yes	Yes	Yes	Yes	Yes
Bit Width	3	2	2	1	1	1	3
Independent Reconfigurability	No	No	No	No	No	Yes	Yes
Angular Range	0-60°	Not provided	Not provided	Not provided	0-30°	Not provided	0-50°

The reflection coefficient spectrum is measured in a microwave anechoic chamber, as shown in Fig. 9. Two horn antennas are symmetrically placed on both sides of the RIS normal to excite and receive EM waves, respectively. A Vector Network Analyzer (VNA, Agilent N5245A) connects the antennas by RF cables. The reflection coefficient can be further obtained by normalizing the reflection signal to that of a metal plate of the same size as the RIS.

Fig. 10 and Fig. 11 show the measurement results at normal incidence and TM 50° oblique incidence, respectively. 3-bit coding can be realized in both FB_1 and FB_2 to achieve independent control of the reflection phase for both normal and oblique incidence. When normally the EM wave incident is on the RIS, the reflection amplitude in FB_1 and FB_2 is greater than –5 dB. While at the incidence of 50°, it shows a slight distortion, which is due to the limited aperture and the truncated boundaries of RIS, as discussed above.

The experimental environment of a scattering pattern measurement is demonstrated in Fig. 12. The RIS and the transmitting antenna are placed on a rotating platform. The transmitting antenna is connected to the analog signal generator (Agilent E8257D) and the receiving antenna is connected to the signal analyzer (Agilent N9010A). When the rotating platform drives the RIS and the transmitting antenna to rotate together, the signal intensity at different receiving angles is measured and recorded. The measured 1D scattering patterns are shown in solid blue lines in Fig. 6 (FB_1) and Fig. 7 (FB_2), demonstrating good agreements with the theoretical and simulated ones.

It should be noted that due to the large incidence angle and the limited RIS aperture, part of the excited EM wave energy is received directly through the line of sight path. The reflection signal superimposes the diffraction signal, which results in ripples in the side lobes of the measured scattering patterns.

Table 2 compares the performance of the proposed RIS element with several early reported RIS designs. Most of the reported dual-band RISs cannot achieve independent modulation of the phase on both bands, except for the one reported in [22]. In addition, the proposed RIS also features a wider bit width and better robustness to the incident angle compared to other work.

5. CONCLUSION

In this paper, a 3-bit RIS with independent control of a phase over dual bands is proposed. By designing two pairs of metal patches of different sizes in one element and loading two varactors on them, independent phase control of the reflected waves in two frequency bands is achieved. The simulation result shows that the induced currents are distributed at different locations in the two frequency bands, which explains the mechanism of independent control of dual-band reflection phases. Numerous metallic vias between adjacent elements are designed to improve the angular stability so that it can perform well in the incident angle range of 0°-50°. The simulation and measurement results of the scattering patterns at normal and oblique incidence are all in good agreement with the theoretical ones. The good performance of the proposed dual-band RIS provides a potential solution to further expand the communication capacity of RIS-based wireless communication systems.

REFERENCES

[1] T. J. Cui, M. Q. Qi, X. Wan et al., “Coding metamaterials, digital metamaterials and programmable metamaterials,” Light: Science & Applications, vol. 3, no. 10, pp. e218-e218, 2014.

[2] S. Liu, T. J. Cui, L. Zhang et al., "Convolution Operations on Coding Metasurface to Reach Flexible and Continuous Controls of Terahertz Beams," Advanced Science, vol. 3, no. 10, 1600156, 2016.

[3] T. J. Cui, S. Liu, and L. L. Li, "Information entropy of coding metasurface," Light: Science & Applications, vol. 5, no. 11, pp. e16172, 2016.

[4] L. Li, T. J. Cui, W. Ji et al., "Electromagnetic reprogrammable coding-metasurface holograms," Nature Communications, vol. 8, no. 1, 197, 2017.

[5] R. Y. Wu, C. B. Shi, S. Liu, W. Wu, and T. J. Cui, "Addition Theorem for Digital Coding Metamaterials," Advanced Optical Materials, vol. 6, no. 5, 1701236, 2018.

[6] T. J. Cui, L. Li, S. Liu et al., "Information Metamaterial Systems," iScience, vol. 23, no. 8, 101403, 2020.

[7] C. Huang, A. Zappone et al., "Reconfigurable Intelligent Surfaces for Energy Efficiency in Wireless Communication," IEEE Transactions on Wireless Communications, vol. 18, no. 8, pp. 4157-4170, 2019.

[8] W. Tang et al., "MIMO Transmission Through Reconfigurable Intelligent Surface: System Design, Analysis, and Implementation," IEEE Journal on Selected Areas in Communications, vol. 38, no. 11, pp. 2683-2699, 2020.

[9] L. Wei, C. Huang et al., "Channel Estimation for RIS-Empowered Multi-User MISO Wireless Communications," IEEE Transactions on Communications, vol. 69, no. 6, pp. 4144-4157, 2021.

[10] Q. Cheng, L. Zhang, J. Dai, W. Tang, J. Ke, S. Liu, J. Liang, S. Jin, T. J. Cui, "Reconfigurable Intelligent Surfaces: Simplified-Architecture Transmitters--From Theory to Implementations," Proceedings of the IEEE, early access, DOI: 10.1109/JPROC.2022.3170498, 2022.

[11] H. L. Wang, H. F. Ma, M. Chen, S. Sun, and T. J. Cui, "A Reconfigurable Multifunctional Metasurface for Full-Space Control of Electromagnetic Waves", Advanced Functional Materials, vol. 31, no. 25, 2100275, 2021.

[12] J. Liang, Q. Cheng et al., "An Angle-Insensitive 3-Bit Reconfigurable Intelligent Surface", IEEE Transactions on Antennas and Propagation, early access, DOI: 10.1109/TAP.2021.3130108, 2021.

[13] J. Ke, J. Dai et al., "Linear and Nonlinear Polarization Syntheses and Their Programmable Controls based on Anisotropic Time-Domain Digital Coding Metasurface," Small Structures, vol. 2, no. 1, 2000060, 2020.

[14] H. Wu, D. Wang et al., "Space-Frequency-Domain Gradient Metamaterials," Advanced Optical Materials, vol. 6, no. 23, 1801086, 2018.

[15] Y. Liang, J. Chen et al., "Reconfigurable intelligent surfaces for smart wireless environments: channel estimation, system design and applications in 6G networks," Science China-Information Sciences, vol. 64, no. 10, Special Issue, 2021.

[16] W. Tang, M. Chen et al., "Wireless Communications with Reconfigurable Intelligent Surface: Path Loss Modeling and Experimental Measurement," IEEE Transactions on Wireless Communications, vol. 20, no. 1, pp. 421-439, 2021.

[17] Y. Saifullah, Q. Chen, G. M. Yang, A. B. Waqas, and F. Xu, "Dual-band multi-bit programmable reflective metasurface unit cell: design and experiment," Optics Express, vol. 29, no. 2, pp. 2658-2668, 2021.

[18] Y. Liu, S. Wang et al., "A Compact Dual-Band Dual-Polarized Antenna with Filtering Structures for Sub-6 GHz Base Station Applications," IEEE Antennas and Wireless Propagation Letters, vol. 17, no. 10, pp. 1764-1768, 2018.

[19] E. Baladi, M. Y. Xu, N. Faria, J. Nicholls, and S. V. Hum, "Dual-Band Circularly Polarized Fully Reconfigurable Reflectarray Antenna for Satellite Applications in the Ku-Band," IEEE Transactions on Antennas and Propagation, vol. 69, no. 12, pp. 8387-8396, 2021.

[20] H. Lin et al., "A dual-band reconfigurable intelligent metasurface with beam steering," Journal of Physics D: Applied Physics, vol. 55, no. 24, 245002, 2022.

[21] H. Yang et al., "A 1600-Element Dual-Frequency Electronically Reconfigurable Reflectarray at X/Ku-Band," IEEE Transactions on Antennas and Propagation, vol. 65, no. 6, pp. 3024-3032, 2017.

[22] N. Zhang et al., "Programmable Coding Metasurface for Dual-Band Independent Real-Time Beam Control," IEEE Journal on Emerging and Selected Topics in Circuits and Systems, vol. 10, no. 1, pp. 20-28, 2020.

[23] B. Liu, Y. He, S. W. Wong, and Y. Li, "Multifunctional Vortex Beam Generation by a Dynamic Reflective Metasurface," Advanced Optical Materials, vol. 9, no. 4, 2001689, 2020.

[24] W. Chen, L. Bai, W. Tang, S. Jin, W. X. Jiang, and T. J. Cui, "Angle-Dependent Phase Shifter Model for Reconfigurable Intelligent Surfaces: Does the Angle-Reciprocity Hold?" IEEE Communications Letters, vol. 24, no. 9, pp. 2060-2064, 2020.

[25] N. Yu, P. Genevet, M. Kats et al., "Light Propagation with Phase Discontinuities: Generalized Laws of Reflection and Refraction," Science, vol. 334, no. 6054, pp. 333-337, 2011.

[26] L. Zhang et al., "Breaking Reciprocity with Space-Time-Coding Digital Metasurfaces," Advanced Material, vol. 31, no. 41, 1904069, 2019.

AUTHORS

Jing Cheng Liang received a B. E. degree from the School of Electronic Science and Engineering, Nanjing University of Posts and Telecommunications, Nanjing, China, China, in 2016, and an M.E. degree from the School of Electronic Science and Engineering, University of Electronic Science and Technology of China, Chengdu, China, in 2019. He is currently working towards his Ph. D. degree at State Key Laboratory of Millimeter Waves, Southeast University, Nanjing, China. His current research interests include metasurfaces, Reconfigurable Intelligent Surfaces (RISs) and the time-reversal method.

Wen Hua Gao received a B. E. degree in electronic information engineering from Xidian University, Xi'an, China, in 2019, and an M. E. degree in electronics and communication engineering at the State Key Laboratory of Millimeter Waves, Southeast University, Nanjing, China, in 2022. Her research interests include metasurfaces and Reconfigurable Intelligent Surfaces (RISs).

Jun Yan Dai received a B.S. degree in information engineering from Southeast University, Nanjing, China, in 2013, and a Ph.D. degree in electromagnetic field and microwave technology from the State Key Laboratory of Millimeter Waves, Southeast University, Nanjing, China, in 2019. From February 2020 to December 2021, he was a postdoctoral fellow with the State Key Laboratory of Terahertz and Millimeter Waves, City University of Hong Kong, Hong Kong. He is currently an associate professor with the State Key Laboratory of Millimeter Waves, Southeast University, Nanjing, China. His research interests include metasurfaces, reconfigurable intelligent surfaces, space-time modulation technology, and wireless communication systems.

Peng Zhang received a bachelor's degree from Harbin Institute of Technology, Harbin, China, in 1994, a master's degree from Tsinghua University, Beijing, China, in 2007, and a Ph.D degree from China Academy of Aeronautics and Astronautics, Beijing, China, in 2017.

He is currently a distinguished professor of Southeast University, Harbin Institute of Technology, Dalian University of Technology. He is the laboratory chief from Aeronautical Science and technology Key Laboratory of Stealth Technology, and Liaoning Key laboratory of Electromagnetic and Optics. He is the chief expert of Aviation Industry Corporation of China, an academic member of the metamaterials Committee of China, and the organizing committee of the High-level Forum on Electromagnetic Security for Infrastructure Networks.

Qiang Cheng (M'15) received B.S. and M.S. degrees from Nanjing University of Aeronautics and Astronautics, Nanjing, Jiangsu, China, in 2001 and 2004 respectively, and a Ph.D. degree from Southeast University, Nanjing, in 2008.

In 2008, he joined the State Key Laboratory of Millimeter Waves, Southeast University, where he was involved in the development of metamaterials and metadevices. He is currently a full professor with the Radio Department, Southeast University. He leads a group of Ph.D. students and master students in the area of metamaterials, tunable microwaves circuits, microwave imaging, and terahertz systems. He has authored or co-authored more than 100 publications, being cited over 2000 times.

Dr. Cheng was a recipient of the 2010 Best Paper Award from the New Journal of Physics, China's Top Ten Scientific Advances of 2010, and the Second Class National Natural Science Award in 2014. He served as the vice chair for the 2008 and 2010 International Workshop on Metamaterials, Nanjing, China.

Tie Jun Cui (M'98–SM'00–F'15) received B.Sc., M.Sc., and Ph.D. degrees in electrical engineering from Xidian University, Xi'an, China, in 1987, 1990, and 1993 respectively. In March 1993, he joined the Department of Electromagnetic Engineering, Xidian University, and was promoted to an associate professor in November 1993. From 1995 to 1997 he was a research fellow with the Institut fur Hochstfrequenztechnik und Elektronik (IHE) at University of Karlsruhe, Germany. In July 1997 he joined the Center for Computational Electromagnetics, Department of Electrical and Computer Engineering, University of Illinois at Urbana-Champaign, first as a postdoctoral research associate and then a research scientist. In September 2001, he was a Cheung-Kong Professor with the Department of Radio Engineering, Southeast University, Nanjing, China. Currently he is Chief Professor of Southeast University, the Director of State Key Laboratory of Millimeter Waves, and Founding Director of the Institute of Electromagnetic Space, Southeast University.

Dr. Cui's research interests include metamaterials and computational electromagnetics. He proposed the concepts of digital coding and programmable metamaterials, and realized their first prototypes, based on which he founded the new direction of information metamaterials, bridging the physical world and digital world. Dr. Cui is the first author of books Metamaterials – Theory, Design, and Applications (Springer, Nov. 2009); Metamaterials: Beyond Crystals, Noncrystals, and Quasicrystals (CRC Press, Mar. 2016); and Information Metamaterials (Cambridge University Press, 2021). He has published over 500 peer-reviewed journal papers, which have been cited more than 44600 times (H-Factor 107; Google Scholar), and licensed over 100 patents. Dr. Cui was awarded a research fellowship from the Alexander von Humboldt Foundation, Bonn, Germany, in 1995, received a Young Scientist Award from the International Union of Radio Science in 1999, was awarded a Cheung Kong Professor by the Ministry of Education, China, in 2001, and received the National Science Foundation of China for Distinguished Young Scholars in 2002. Dr. Cui received the Natural Science Award (first class) from the Ministry of Education, China, in 2011, and the National Natural Science Awards of China (second class, twice), in 2014 and 2018 respectively. His research has been selected as one of the most exciting peer-reviewed optics research "Optics in 2016" by Optics and Photonics News Magazine, 10 Breakthroughs of China Science in 2010, and many research highlights in a series of journals. His work has been widely reported by Nature News, MIT Technology Review, Scientific American, New Scientists, Discover, etc.

Dr. Cui is the Academician of Chinese Academy of Science, and IEEE Fellow. He served as an associate editor of IEEE Transactions on Geoscience and Remote Sensing, and as a guest editor of Science China - Information Sciences, Science Bulletin, IEEE JETCAS, Engineering, and Research. Currently he is the chief editor of Metamaterial Short Book Series in Cambridge University Press, the editor of Materials Today Electronics, the associate editor of Research, and an editorial board member of National Science Review, eLight, PhotoniX, Advanced Optical Materials, Small Structure, and Advanced Photonics Research. He has presented more than 100 keynote and plenary talks in academic conferences, symposiums, and workshops. From 2019 to 2021, he was ranked in the top 1% for the highly cited papers in the field of physics by Clarivate Web of Science (Highly Cited Researcher).